A&A 395, 647–656 (2002)
DOI: 10.1051/0004-6361:20021180

Astronomy & Astrophysics

The time-dependent ejection velocity histories of HH 34 and HH 111

A. C. Raga[1], P. F. Velázquez[1], J. Cantó[2], and E. Masciadri[2]

[1] Instituto de Ciencias Nucleares, UNAM, Ap. 70-543, 04510 D.F., México
e-mail: pablo@nuclecu.unam.mx
[2] Instituto de Astronomía, UNAM, Ap. 70-264, 04510 D.F., México
e-mail: elena@astroscu.unam.mx

Received 24 May 2002 / Accepted 31 July 2002

Abstract. The southern lobe of HH 34 and the western lobe of HH 111 show remarkable similarities. Both objects have a chain of well aligned knots, ending in well defined bow shocks (HH 34S and HH 111V, respectively). In this paper, we derive the past ejection velocity histories from previously published radial velocity measurements of the HH 34 and HH 111 jets. This is done under the assumption that the flows are ballistic. From these reconstructed ejection velocity variabilities, we compute axisymmetric gasdynamic simulations of the two flows, and find that we do obtain large working surfaces at the positions of the HH 34S and HH 111V bow shocks for the time at which these objects are being observed. This appears to be quite definite proof that these bow shocks are indeed the result of an ejection velocity time-variability. Also, there is the observational fact that the HH 34S bow shock is huge, being wider than HH 111V by a factor of ∼3. We find that we can reproduce this difference in size by choosing an appropriate value for the density of the ambient medium. Finally, from our small sample of two reconstructed ejection velocity variability histories, we attempt to make some statements about the general nature of these variabilites, and their implications on the possible ejection/collimation mechanisms.

Key words. ISM: Herbig-Haro objects – ISM: jets and outflows – ISM: kinematics and dynamics – ISM: individual objects: HH 34, HH 111 – shock waves

1. Introduction

The HH 34 and HH 111 flows are among the best studied of all HH outflows. Since their discoveries (Reipurth et al. 1986 and Reipurth 1989, respectively), detailed spectroscopic, imaging and proper motion studies of these objects have been carried out at optical wavelengths (HH 34: Bührke et al. 1998; Reipurth & Heathcote 1992; Eislöffel & Mundt 1992; Heathcote & Reipurth 1992; Morse et al. 1992; Morse et al. 1993a; HH 111: Reipurth et al. 1992; Noriega-Crespo et al. 1993; Morse et al. 1993a,b; Riera et al. 2001) and recently, these studies have been complemented with HST data (HH 34: Reipurth et al. 2002; HH 111: Reipurth et al. 1997a; Hartigan et al. 2001; Raga et al. 2002a). A wealth of infrared (Gredel & Reipurth 1994; Davis et al. 1994; Coppin et al. 1998; Reipurth et al. 1999; Reipurth et al. 2000; Davis et al. 2001) as well as radio data (Cernicharo & Reipurth 1996; Nagar et al. 1997; Reipurth et al. 1999) also been obtained.

In discussing these objects, we should also mention that HH 34 and HH 111 represent the central regions of systems of "giant jets" or "parsec scale jets". These spatially very extended systems of HH objects have been described in considerable detail in the recent literature (see, e.g., Bally & Devine 1994; Eislöffel & Mundt 1997; Devine et al. 1997; Reipurth et al. 1997b; Rosado et al. 1999).

The popularity of HH 34 and HH 111 arises from the fact that the southern lobe of the HH 34 outflow and the western lobe of HH 111 represent the best examples of jet-like HH flows. These two jets have quite remarkable similarities. Both of the objects show a chain of well aligned knots close to the source (i.e., at distances of up to ∼50″), and have well defined "heads" (HH 34S and HH 111V) at a distance of ∼100–150″ from the source.

Even though the heads of both objects show bow shock-like morphologies, they have surprisingly different sizes: HH 111V has a full width of ∼10″, while HH 34S is ∼30″ wide! This difference does not reflect a difference in the diameters of the jets, since the HH 34 jet is actually somewhat narrower than the HH 111 jet (∼0.″5 for HH 34 vs. ∼0.″7 for HH 111, see Reipurth et al. 2002 and Hartigan et al. 2001).

In order to investigate whether the HH 34S and HH 111V bow shocks are the result of a time-variability of the source, we have first attempted to deduce the ejection velocity variability that gave rise to these objects from the radial velocity data of Heathcote & Reipurth (1992) and Reipurth et al. (1997). This process is described in detail in Sect. 2.

Send offprint requests to: A. Raga,
e-mail: raga@astroscu.unam.mx

With the reconstructed ejection velocity histories, we then compute axisymmetric gasdynamic simulations of the jet flows, and obtain predictions of the appearance of the HH 34 and HH 111 jets corresponding to the present time. With these simulations we try to understand the differences between HH 34S and HH 111V. The results obtained from this exercise are discussed in Sect. 3.

A somewhat similar approach was used by Raga & Noriega-Crespo (1998), who used the separation between knots and proper motion measurements in order to deduce the existence of three modes in the ejection velocity variability history of HH 34. These authors found that a gasdynamic simulation computed with this variability did reproduce the morphology of HH 34 in a quite successful way.

Our present approach, based on radial velocity measurements, was previously used for the HH 46/47 outflow by Raga et al. (1990), and allows us to find the phase, as well as the period and amplitude of the modes. This gives us a more detailed reconstruction of the ejection velocity history of the objects than the one obtained by Raga & Noriega-Crespo (1998, who did not try to derive the relative phases between the three modes of HH 34). Also, we are able to evaluate to what extent sinusoidal modes are actually appropriate for describing the time-variability of the ejection of HH jets.

Recently, Raga et al. (2002a) and Masciadri et al. (2002) have used HST long-slit spectra to derive the ejection velocity history of HH 111. However, these studies were limited to the analysis of the three brighter knots along the HH 111 jet, and therefore only gave a short period mode appropriate for modelling the chain of knots close to the source. In the present paper, we extend the study of the ejection time-variability to search for longer period modes, which are necessary for explaining the larger bow shocks such as HH 111V.

Finally, we use the reconstructed ejection velocity variability histories of HH 111 and HH 34 in order to speculate about the nature of the ejection mechanisms for HH jets in general. This somewhat risky endeavour is described in Sect. 4.

We should point out that the present study, which is based on radial velocity measurements, is in principle equivalent to the study of HH 34 carried out by Raga & Noriega-Crespo (1998), which was based on proper motion measurements. The equivalence between the two approaches is seen in the fact that the results that we obtain in this paper for HH 34 are indeed very similar to the ones obtained by Raga & Noriega-Crespo (1998).

2. The ejection velocity histories of HH 34 and HH 111

As described in Raga et al. (1990), for a hypersonic, quasi-ballistic jet, it is possible to reconstruct the past ejection velocity time-variability from the observed kinematical structure of the flow. From the observed axial velocity $v(z)$ of the jet (as a function of distance z from the source) observed at $t = 0$ (i.e., at the current time), one can compute the dynamical time $t = -z/v(z)$ at which the ballistic fluid parcels were ejected from the source. One can then compute the past ejection velocity history of the jet as $v_j(t) = v[t = -z/v(z)]$. We have carried out this simple process for the HH 34 and HH 111 jets.

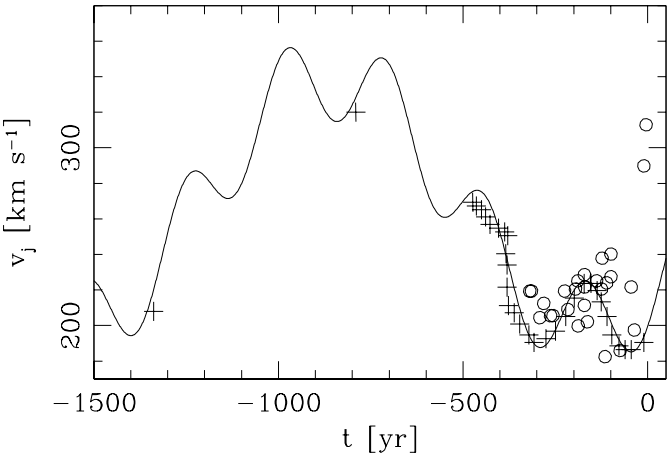

Fig. 1. Ejection velocity as a function of time ($t = 0$ being the present time) reconstructed from the radial velocities (crosses, taken from Heathcote & Reipurth 1992) and proper motions (circles, taken from Reipurth et al. 2002) of HH 34. The distances and velocities have been deprojected assuming a $\phi = 30°$ angle between the outflow axis and the plane of the sky. The point at $t \approx -800$ yr has been calculated with the radial velocity upstream of HH 34S, and the point at $t \approx -1330$ yr corresponds to the flow velocity immediately downstream of this bow shock. A two-mode fit to the ejection velocity variability is also shown.

For HH 34, we have taken the radial velocity measurements of Heathcote & Reipurth (1992) for the knots along the jet. We have deprojected the distances from the source and the radial velocities considering an angle $\phi = 30°$ between the outflow axis and the plane of the sky, in order to find the spatial velocity $v(z)$ as a function of distance z from the source (also considering a distance of 460 pc to HH 34). From these radial velocities, we compute the dynamical time as a function of position (see above), and then plot the jet velocity as a function of dynamical time to obtain the reconstructed ejection velocity time-variability $v_j(t)$. The result obtained from this exercise is shown in Fig. 1.

In this figure, we also show the velocity vs. dynamical time dependence obtained from the HST proper motions of HH 34 obtained by Reipurth et al. (2002). These measurements appear to give a larger scatter, which could be partially due to larger errors in the velocities derived from the proper motions. Also, there are intrinsic uncertainties in deriving proper motions from knots which change shape as they travel away from the source, leading to a lack of determination as to what these velocities are telling us in detail (see Biro 1996).

Because of their better behaviour (see Fig. 1), we concentrate on the $v_j(t)$ derived from the radial velocity data. To the points derived from the observations, we carry out an unweighted, least squares fit with a function of the form :

$$v_j(t) = v_0 + v_1 \sin(2\pi t/\tau_1 + \phi_1) + v_2 \sin(2\pi t/\tau_2 + \phi_2)\,, \qquad (1)$$

and obtain a mean velocity $v_0 = 270$ km s^{-1}, a first mode with $v_1 = 70$ km s^{-1}, $\tau_1 = 1400$ yr and $\phi_1 = -0.80$ rad, and a second mode with $v_2 = 25$ km s^{-1}, $\tau_2 = 270$ yr and $\phi_2 = -0.85$ rad.

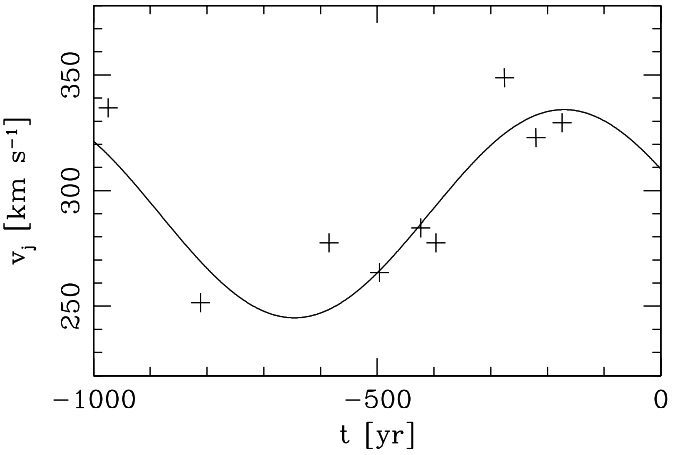

Fig. 2. Ejection velocity as a function of time ($t = 0$ being the present time) reconstructed from the radial velocities of HH 111 (crosses, taken from Reipurth et al. 1997a). The distances and velocities have been deprojected assuming a $\phi = 11^\circ$ angle between the outflow axis and the plane of the sky. A single-mode, sinusoidal fit to the ejection velocity variability is also shown.

From Fig. 1, it is clear that a reasonably good fit is obtained to the data.

These two modes are very similar to the two longer period modes deduced through other arguments by Raga & Noriega-Crespo (1998). However, these authors also determined a third, shorter period mode from the separation of the successive knots in the base of the HH 34 jet. In the ground based spectroscopic data of Heathcote & Reipurth (1992), we do not see the velocity variabilities associated with these closely spaced knots.

In order to have a model for the HH 34 jet that also has a chain of knots close to the source (such as the one observed in this object), we then also include the third mode determined by Raga & Noriega-Crespo (1998):

$$v_3 \sin(2\pi t/\tau_3)\,, \tag{2}$$

with $v_3 = 10$ km s^{-1}, $\tau_3 = 27$ yr, and add it to the variability determined from the radial velocity data (Eq. (1)). We do not have a determination of the relative phase of this third mode.

Contrary to the first two modes (see Eq. (1)), for which the radial velocity data show evidence that a sinusoidal shape is indeed appropriate (see Fig. 1), there is no observational evidence that this third mode (Eq. (2)) also has such a shape. Raga & Noriega-Crespo (1998) only derived a period and an amplitude from the properties of the knots close to the HH 34 source, and then assumed that these parameters are associated with a sinusoidal ejection velocity mode. Due to the lack of new observational constraints, here we adopt the assumed sinusoidal mode of Raga & Noriega-Crespo (1998).

For HH 111, we take the radial velocity data of Reipurth et al. (1997a), deproject the velocities and distances assuming a $\phi = 11^\circ$ angle between the outflow axis and the plane of the sky, and then compute the ejection velocity time-variability as described above. The results of this exercise are shown in Fig. 2.

From this figure, it is apparent that the ejection velocity time-variability is simpler, and can be fitted with a single sinusoidal mode. With a least squares fit with a functional form

$$v_j(t) = v_a + v_b \sin(2\pi t/\tau_b + \phi_b)\,, \tag{3}$$

we obtain $v_b = 290$ km s^{-1}, $v_b = 45$ km s^{-1}, $\tau_b = 950$ yr and $\phi_b = 2.7$ rad. This fit is shown superposed on the data in Fig. 2.

Again, in the radial velocity data, we do not see the velocity variations associated with the knots in the chain at the base of HH 111. For these knots, we use the velocity variability deduced from HST long-slit spectroscopy by Raga et al. (2002a) and Masciadri et al. (2002). These authors deduced a sawtooth variability of the form

$$\{t - \tau_c \times [1/2 + \text{Integer}\,(t/\tau_c)]\}\; v_c\,, \tag{4}$$

with $v_c = 60$ km s^{-1} and $\tau_c = 60$ yr. We then simply add this mode to the ejection velocity variability deduced from the ground based radial velocity data (see Eq. (3)) in order to obtain a two-mode description.

In the following section, we describe axisymmetric gasdynamic simulations carried out with the ejection velocity time-variability of HH 34 described by Eqs. (1) and (2), and with the one of HH 111 given by Eqs. (3) and (4).

3. Gasdynamical simulations

3.1. General description

We have carried out numerical simulations with the two ejection velocity variabilities discussed in Sect. 2 using an axisymmetric version of the yguazú-a adaptive grid code. This code has been described in detail by Raga et al. (2000), and has been extensively tested with laboratory experiments of explosions (Sobral et al. 2000; Velázquez et al. 2001) and jets (Raga et al. 2001). The version of the yguazú-a code that we have employed integrates the gasdynamic equations with the "flux vector splitting" algorithm of van Leer (1982), together with a system of rate equations for atomic/ionic species.

Rate equations for H I, H II, He I, He II, He III, C II, C III, C IV, O I, O II, O III and O IV are integrated, and a non-equilibrium cooling function is computed with these species. The reaction and cooling rates which have been included are described in detail by Raga et al. (2002).

The HH 34 and HH 111 simulations were carried out in a computational domain of $(16.8, 2.1) \times 10^{17}$ cm along the axial and radial coordinates. A four-level binary adaptive grid with a maximum resolution of 1.64×10^{15} cm (along both axes) was employed. The jet is injected at $z = 0$, and a reflection condition is applied on the $z = 0$ plane outside of the jet beam as well as on the symmetry axis. A free outflow condition is applied on the other two grid boundaries.

For both simulations, we have chosen a $r_j = 10^{16}$ cm initial jet radius, and a time-independent jet number density $n_j = 5000$ cm^{-3} and temperature $T_j = 1000$ K. The environment is homogeneous, with density $n_{env} = 15$ cm^{-3} (for the HH 34 simulation) or $n_{env} = 100$ cm^{-3} (for the HH 111 simulation) and temperature $T_{env} = 1000$ K. Both the jet and the

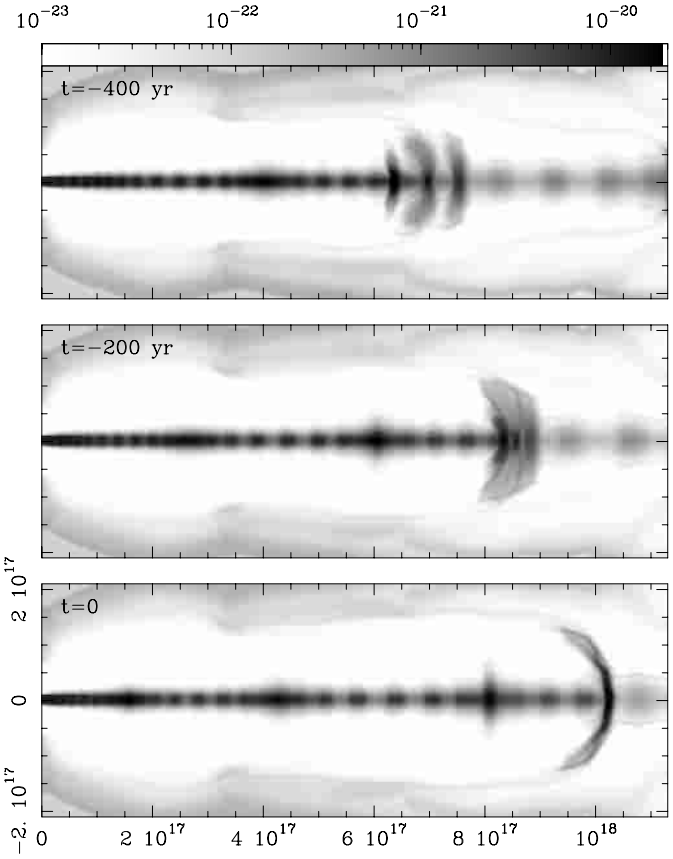

Fig. 3. Time sequence of the density stratifications obtained from the HH 34 model. The simulation is started at $t = -3000$ yr, and $t = 0$ corresponds to the time at which HH 34 is being observed. The densities are depicted with a logarithmic greyscale, with the values given (in g cm^{-3}) by the bar on the top of the figure. The z (horizontal) and r (vertical) axes are labeled in cm. The computational domain extends out to $z = 1.68 \times 10^{18}$ cm.

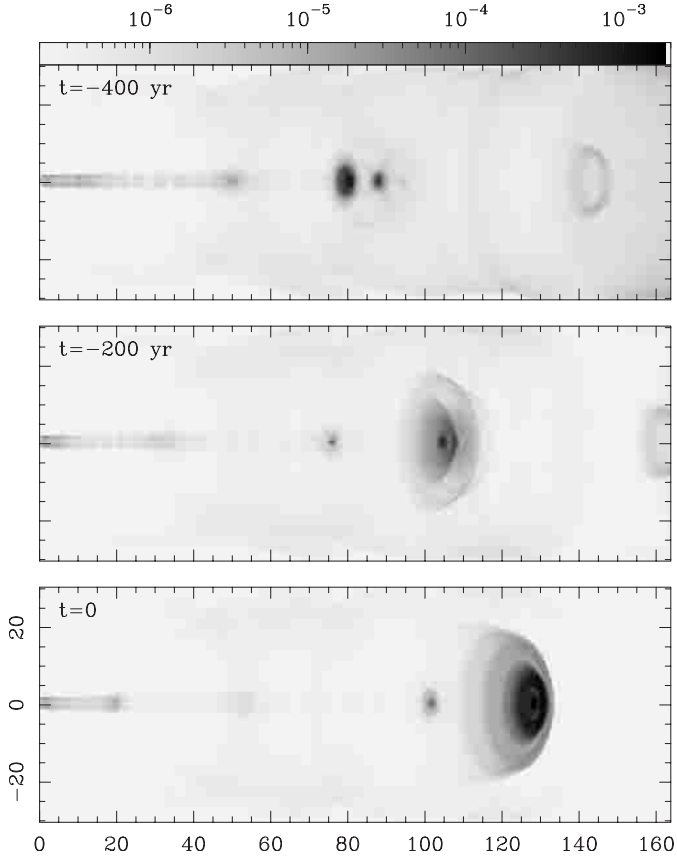

Fig. 4. Time sequence of the Hα maps predicted from the HH 34 model. The simulation is started at $t = -3000$ yr, and $t = 0$ corresponds to the time at which HH 34 is being observed. The maps have been computed assuming a $\phi = 30°$ angle between the outflow axis and the plane of the sky. The Hα intensities are depicted with a logarithmic greyscale, with the values given (in erg s^{-1} cm^{-2} sterad^{-1}) by the bar on the top of the figure. The x (horizontal) and y (vertical) plane of the sky coordinates are labeled in arcsec (computed as offsets from the position of the source assuming a distance of 460 pc to the object).

environment are initially neutral, with the exception of carbon, which is singly ionized.

The assumption of a homogeneous environment is of course not very realistic for modelling HH objects, which emerge from a dense region surrounding the outflow source, into a more diffuse environment. This is particularly true for the case of HH 111, in which a high extinction region of $\sim 3 \times 10^{17}$ cm surrounding the source is observed (see, e.g., Reipurth et al. 1992). However, the introduction of a stratified environment, and a study of the effects that it has on the structure of the HH jets, is left for a future paper.

The time-integrations carried out with the ejection velocity variabilities deduced for HH 34 and HH 111 are described in the following two subsections.

3.2. HH 34

Using the setup described in Sect. 3.1, we have computed a model for HH 34, using the ejection velocity time-variability given by Eqs. (1) and (2). We start the numerical simulation at $t = -3000$ yr, and integrate forward in time until $t = 0$, corresponding to the present time, at which HH 34 is being observed.

Figure 3 shows a time-sequence of the density stratification over the last 400 years of the time-integration. It is clear that around this time the jet flow is in a very particular phase of its evolution. Between $t = -200$ yr and $t = 0$, three working surfaces of mode 2 (see Eq. (1)) merge together. This merging takes place because the flow in this region is steepening to form a mode 1 working surface.

Figure 4 shows the Hα intensity maps predicted for the same three time frames as Fig. 3. These maps have been calculated assuming a $\phi = 30°$ angle between the outflow axis and the plane of the sky. At $t = 0$, we see a large, bow shaped structure which qualitatively resembles HH 34S, with its leading edge at a distance of $\approx 9 \times 10^{17}$ cm from the source. This distance corresponds to an angular extent of 130″ (at 460 pc), which agrees well with the 110″ distance from the leading edge of HH 34S to the outflow source (see, e.g., Fig. 9 of Reipurth et al. 2002).

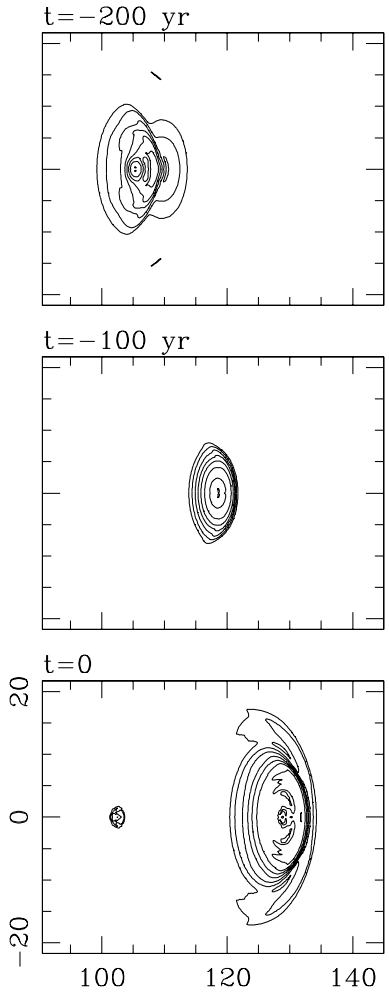

Fig. 5. Time sequence of the Hα maps predicted from the HH 34 model. The maps are depicted with 8 factor of 2, logarithmic contours, with the highest contour corresponding to ∼99% of the peak intensity of each of the displayed maps. The peak intensities have values of 0.77 (top), 6.4 (centre) and 1.87×10^{-3} erg cm^{-2} s^{-1} sterad^{-1} (bottom). The x (horizontal) and y (vertical) plane of the sky coordinates are labeled in arcsec (computed as offsets from the position of the source assuming a distance of 460 pc to the object).

Therefore, one of the main results of our analysis is the following. If, under the assumption of a ballistic flow, one uses the radial velocities along the HH 34 jet to reconstruct the past history of an assumed ejection velocity time-variability, and then integrates a jet simulation with this variability up to the present time, one obtains an intensity map with a dominant, bow shaped structure at the approximate position of HH 34S. We believe that this is the most convincing proof up to now that HH 34S is indeed the result of an ejection velocity variability.

In the computed Hα maps, one sees a quite dramatic change in the morphology of the three merging working surfaces. In the merging process, a wide bow shock is formed. In order to evaluate the width of this bow shock, in Fig. 5 we have plotted the region around the merging working surfaces as logarithmic contour plots. In these plots, the faintest contour corresponds to a factor of 1/128 of the maximum intensity of each map, approximately corresponding to the dynamical range of typical observations of HH 34S.

In the $t = 0$ map of Fig. 5 (corresponding to the time at which HH 34 is being observed), one sees a bow shaped structure with a bright, inner region with a full width of $\approx 1.5 \times 10^{17}$ cm (corresponding to $\approx 22''$ at 460 pc) and faint wings extending out to a full width of $\approx 2.4 \times 10^{17}$ cm ($\approx 35''$ at 460 pc). These values are in very good agreement with the $30''$ full width measured for HH 34S (see Sect. 1 and Reipurth et al. 2002).

Interestingly, the HST images show that HH 34S has an outer, higher excitation bow shock, and inner, lower excitation bow shaped structure (Reipurth et al. 1997a, Fig. 18). Reipurth et al. (2002) find that the proper motions of this inner structure (corresponding to their cross correlation boxes number 1, 2, 3 and 4) are high (including the highest proper motion of all of the cross correlation boxes covering HH 34S), and appears to be catching up with the leading bow shock. Therefore, one might actually be seeing a merger between successive working surfaces currently taking place within the complex structures observed in HH 34S.

3.3. HH 111

Using the setup described in Sect. 3.1, we have computed a model for HH 111, using the ejection velocity time-variability given by Eqs. (3) and (4). We start the numerical simulation at $t = -2000$ yr, and integrate forward in time until $t = 0$, corresponding to the present time, at which HH 111 is being observed.

Figure 6 shows a time-sequence of the density stratification over the last 400 years of the time-integration. In the three frames, we see a chain of knots close to the source (resulting from the mode given by Eq. (4)), as well as a large working surface (which results from the mode given by Eq. (3)).

These structures are also seen in the predicted Hα maps (computed assuming a $\phi = 11^\circ$ angle between the outflow axis and the plane of the sky, see Fig. 7). The $t = 0$ frame of Fig. 7 shows that the leading edge of the main bow shock has reached a distance of $\approx 1.2 \times 10^{18}$ cm from the source at the time at which we are observing HH 111. This distance corresponds to $174''$ at a distance of 460 pc, in good agreement with the $150''$ between the leading edge of HH 111V and the outflow source (see Fig. 10 of Reipurth et al. 1997a).

Therefore, we conclude that if we take the observed radial velocity vs. position measured along the HH 111 jet, and interpret it as being the result of a time-dependence in the ejection, we end up with a jet model which does produce a main bow shock at the approximate position of HH 111V. This result is completely consistent with what we have found for the HH 34 outflow (see Sect. 3.2).

In Fig. 8, we show a contour plot of the main working surface of the $t = 0$ Hα map (also see Fig. 7). We have used $\sqrt{2}$ logarithmic contours, with the lowest contour corresponding to 1/8 of the peak intensity. This dynamical range is identical to the one of Fig. 18 of Reipurth et al. (1997a), in which HH 111V has a $\approx 10''$ full width (measured perpendicular to

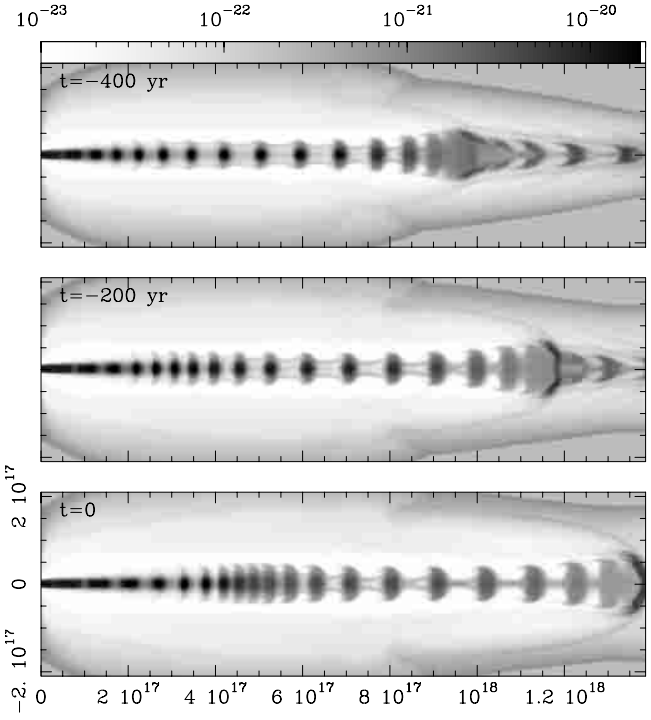

Fig. 6. Time sequence of the density stratifications obtained from the HH 111 model. The simulation is started at $t = -2000$ yr, and $t = 0$ corresponds to the time at which HH 111 is being observed. The densities are depicted with a logarithmic greyscale, with the values given (in g cm^{-3}) by the bar on the top of the figure. The z (horizontal) and r (vertical) axes are labeled in cm. The computational domain extends out to $z = 1.68 \times 10^{18}$ cm.

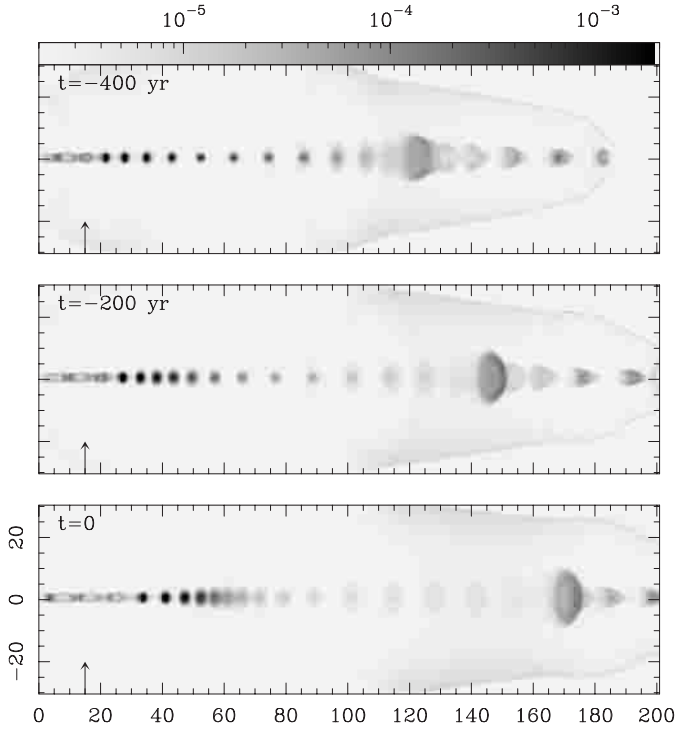

Fig. 7. Time sequence of the Hα maps predicted from the HH 111 model. The simulation is started at $t = -2000$ yr, and $t = 0$ corresponds to the time at which HH 111 is being observed. The maps have been computed assuming a $\phi = 11°$ angle between the outflow axis and the plane of the sky. The Hα intensities are depicted with a logarithmic greyscale, with the values given (in erg s^{-1} cm^{-2} sterad^{-1}) by the bar on the top of the figure. The x (horizontal) and y (vertical) plane of the sky coordinates are labeled in arcsec (computed as offsets from the position of the source assuming a distance of 460 pc to the object). The vertical arrows at $x = 15''$ indicate the position at which the HH 111 jet becomes visible, as it exits the high extinction region in which the outflow source is embedded.

the outflow axis). From our Fig. 8, we measure a full width of $\approx 1.1 \times 10^{17}$ cm (corresponding to 16″ at a distance of HH 111) which is somewhat too wide compared to HH 111V.

We find that in the numerical simulations, the width of the main working surface is strongly dependent on the value chosen for the density of the ambient medium. As an example, in Fig. 8 we show the $t = 0$ Hα map predicted from a model identical to the HH 111 model described in Sect. 3.1, but with a $n_{\rm env} = 15$ cm^{-3} ambient density (rather than the $n_{\rm env} = 100$ cm^{-3} value chosen in Sect. 3.1). This model results in a full width of $\approx 1.5 \times 10^{17}$ cm for the main bow shock, which is actually similar to the width that we found for the main working surface of the HH 34 jet model (which also had a $n_{\rm env} = 15$ cm^{-3} ambient density, see Sects. 3.1, 3.2).

This result is not surprising, as previous studies have shown that the transverse extent of internal working surfaces does depend on the density of the material surrounding the jet beam (Falle & Raga 1993, 1995). Therefore, we conclude that the transverse extents of HH 34S and HH 111V are sensitive not only to the ejection velocity time-variability, but also to the properties of the medium surrounding the jet.

4. Discussion

4.1. Ejection velocity histories

In this paper, we have taken previous observations of radial velocities as a function of position along the HH 111 and HH 34 jets, and interpreted them as the result of a time-dependent ejection velocity variability. Assuming that the flows are ballistic, the radial velocities can be used to reconstruct the history of the ejection velocity over the past ≈1000 yr for the jet segment between HH 111V and the source, and for the past ≈1300 yr from the jet segment between HH 34S and the source.

4.2. HH 34

We find that the reconstructed HH 34 ejection velocity variability can be fitted with two sinusoidal modes and a 270 km s^{-1} mean velocity. Most evident in the measurements is a mode with a period of 270 yr and half-amplitude of 25 km s^{-1}. One and a half periods of this mode are clearly evident in the most recent 500 yr of the velocity variability reconstructed from the measured radial velocities (see Fig. 1). From the fit to the data, it is clear that the observations show both the rises and falls of a sinusoidal mode, so that the real velocity variability appears to be appropriately described by such a functional form.

In order to fit the reconstructed ejection velocity history, it is necessary to introduce a second mode, with a period of 1400 yr and a half-amplitude of 70 km s^{-1}. From Fig. 1,

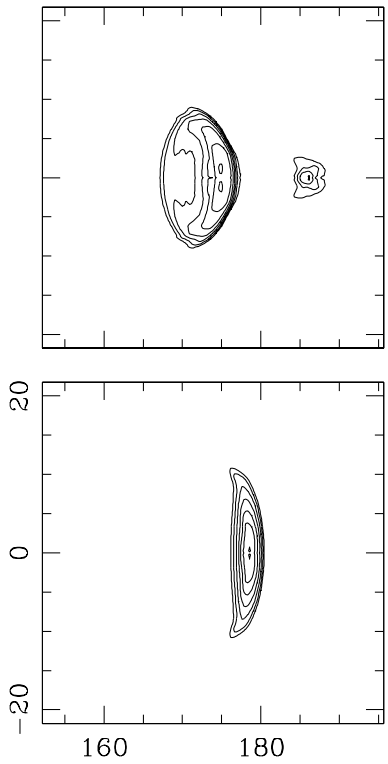

Fig. 8. Hα maps predicted from the HH 111 models with ambient medium number densities of 100 cm^{-3} (top) and 15 cm^{-3} (bottom) for $t = 0$. The maps are depicted with 7 factor of $\sqrt{2}$, logarithmic contours, with the highest contour corresponding to ∼99% of the peak intensity of each of the displayed maps. The peak intensities have values of 1.50 (top) and 2.37×10^{-4} erg cm^{-2} s^{-1} sterad^{-1} (bottom). The x (horizontal) and y (vertical) plane of the sky coordinates are labeled in arcsec (computed as offsets from the position of the source assuming a distance of 460 pc to the object).

it is clear that the general rise in ejection velocity from $t = 0$ to $t = -800$ yr is well fitted by this mode. However, the drop in radial velocity of this mode from $t = -800$ to -1400 yr mostly corresponds to material that has been intercepted by the two shocks of the HH 34S working surface. Therefore, it is not possible to say whether or not this smooth drop in radial velocity is actually present in the real velocity variability with which the HH 34 jet has been ejected.

From this discussion, we see that the kinematics of the HH 34 jet imply that the ejection velocity is varying with time as a superposition of two, smooth modes, for which we can determine the periods, amplitudes and phases. Clearly, no indication of a variability with separate "ejection events" is seen.

To the time-variability deduced from the observed radial velocities, we have added a third, fast mode with a period of 27 yr and a half-amplitude of 10 km s^{-1}. This mode was deduced by Raga & Noriega-Crespo (1998) from the spacing of the knots close to the source of HH 34, and we have included it in order to produce models that have chains of knots similar to these. Even though there is no observational information of the functional form of this mode, we have followed Raga & Noriega-Crespo (1998) in assuming that it is sinusoidal.

Let us now consider the timescales over which these modes have been active. The 1400 yr period mode has clearly been active over the last ∼1000 – 1500 yr. Also, if one attempts to model the knots along the HH 34 giant jet (see Devine et al. 1997), one needs to have a variability with a period of ∼1000 yr. Therefore, the knots along the giant jet might be evidence for the presence of this mode back to ≈10 000 yr ago.

Interestingly, the current time seems to approximately coincide with one of the low velocity "valleys" of the 1400 yr period mode. This mode could either continue existing, so that over the next century we would be seeing a clear rise in the ejection velocity, or it could be that this mode has just died out, and that no such rise will be observed. Interestingly, the HST proper motions of the two knots closest to the HH 34 source appear to be substantially higher than the motions of the other knots (see Fig. 1 and Reipurth et al. 2002), so that we might already be seeing evidence of an increase in the ejection velocity of the HH 34 jet.

The proper motions of the two knots closest to the outflow source (see Fig. 1 and Reipurth et al. 2002) are indeed very intersting. Their values are very high, indicating velocities of ≈300 km s^{-1}, which are similar to the flow velocity directly upstream of HH 34S. As can be seen from Fig. 1, if one includes these velocities when making a fit to the ejection velocity vs. time, one finds that a sinusoidal form for the 1400 yr period mode (mode 1 of Eq. (1)) does not appear to be appropriate. These high proper motions for the knots closest to the outflow source might then be giving us an indication that the long period mode of the HH 34S outflow is actually not sinusoidal. Alternatively, they could be evidence for the existence of a fourth mode, which we have not detected in our present analysis.

We appear to be observing the 270 yr mode also at its minimum (again calling into question whether or not it will extend into the future), but we do appear to see that the 27 yr period mode is still active at the present time (as the chain of aligned knots along the jet starts right by the position of the source). We also see evidence that these two modes have existed at least for the last 500 yr (see Fig. 1). We do not know whether or not these modes have existed further into the past, and it is not clear whether it will ever be possible to retrieve such information from the observed structure of the HH 34 jet.

4.3. HH 111

We find that it is possible to fit the ejection velocity history of HH 111 with a single sinusoidal mode and a mean velocity of 290 km s^{-1}. This mode has a 950 yr period and a 45 km s^{-1} half-amplitude.

In order to produce the chain of aligned knots at the base of the HH 111 jet, it is necessary to introduce a second, shorter period mode. Raga et al. (2002a) and Masciadri et al. (2002) have analyzed long-slit spectroscopic data obtained with the HST, and have concluded that these knots are formed by a "sawtooth" mode (with approximately linear ramps of increasing velocity vs. time followed by sudden drops) with a 60 yr period and 30 km s^{-1} half-amplitude. We have then included this mode in our numerical simulation of HH 111.

The radial velocities of HH 111 show that 950 yr mode has been active over the past 1500 yr (see Fig. 2). Also, the existence of the HH 111 giant jet (see Reipurth et al. 1997b) is evidence that this mode could have been active for ∼10 000 yr. Different from what we found for HH 34, in the observations of HH 111 we are catching the longer period mode close to its peak velocity. Therefore, in this object there is no doubt that the longer period mode is still alive and healthy, and that it coexists in time with the shorter period mode.

The 60 yr period mode has been active over the past ∼500 yr (corresponding to the dynamical timescale of the chain of aligned knots at the base of the HH 111 jet).

4.4. Periods, amplitudes and shock velocities

It is clear that the five modes deduced for the HH 34 and HH 111 jets have monotonically growing amplitudes for increasing periods. This is a simple property that will have to be satisfied by future models of time-dependent ejection mechanisms for these two HH jets.

We find that the mean velocities of HH 34 and HH 111 are uncannily similar to each other (270 and 290 km s^{-1}, respectively). Also, the full amplitudes of the modes have a maximum value of 140 km s^{-1} (this value being attained by the 1400 yr mode of HH 34). From this, we see that the ratios between the half-amplitudes and the mean velocity have a maximum value of $\Delta v/v_j \sim 1/4$. This result shows that the $\Delta v/v_j \sim 1$ "hammer jet" model proposed for HH 111 and HH 34 by Völker et al. (1999) does not appear to be correct.

The maximum amplitude found for the modes of the ejection velocity variability is interesting from the point of view of the possible shock velocities determining the excitation of the spectra of HH objects. With the possible exception of HH 80/81 (see Heathcote et al. 1998), high excitation HH objects are well modeled with shock velocities between 80 and 120 km s^{-1}. The existence of a maximum shock velocity (as deduced from the observed line ratios) lead Raga et al. (1996) to speculate whether there might be problems with the predictions from plane-parallel, steady shock models, and to suggest that these models might be missing other effects which could be present in the excitation of HH spectra.

Interestingly, the velocity variability amplitudes deduced from the radial velocities of HH 34 and HH 111 are indeed consistent with the upper limit for the shock velocities deduced from the excitation of HH spectra. Therefore, it appears that the spectra predicted by plane shock models might be correct, and that the ∼120 km s^{-1} upper limit to the shock velocities then corresponds to an intrinsic property of the amplitudes of the ejection velocity variabilities of HH jets.

In other words, from this interpretation of the excitation of HH spectra, we would conclude that there is an upper limit to the amplitudes of the modes (corresponding to a full amplitude of ∼200 km s^{-1}, which could be divided into two working surface shocks of ∼100 km s^{-1}). This is a second property which should be satisfied by models of the ejection of variable jets.

A third property that has to be satisfied by the jet production mechanism is that several modes appear to coexist in time. For example, Reipurth (2000) suggested that the variability of HH jets might be due to perturbations of an accretion disk by stellar companions in a disintegrating, multiple system. Looking at this scenario without understanding in detail how the perturbations (due to close passages of companions) lead to a time-variability of the outflow, it appears that it would lead to long period modes being excited as the system is disintegrating (while having orbits with ∼1000 yr periods). After a period of $\sim 10^4$ yr, a close binary would be formed, with a ∼10–50 yr period, leading to the excitation of the faster modes seen in HH jets.

Such a sequence of events is not supported by the observed velocity vs. position structures of HH 34 and HH 111, as they indicate that the faster and slower ejection velocity variability modes occur at the same time. Of course, this result does not necessarily eliminate the scenario proposed by Reipurth (2000). A much more detailed study should be carried out to see if it is not possible for orbits in a disintegrating multiple system to lead to coexisting modes such as are observed in HH 34 and HH 111.

4.5. The functional forms of the modes

From the presently available data, we have clear observational constraints for the shape of only two of the five modes assumed to be present in HH 34 and HH 111:

- the 270 yr mode of HH 34 has smooth rises and decays. A sinusoidal function appears to be appropriate for describing this mode;
- the 60 yr period mode of HH 111 has smooth, approximately linear rises, followed by sudden drops in the ejection velocity. We refer the reader to Raga et al. (2002a) and Masciadri et al. (2002) for analyses of this mode.

These two kinds of variability suggest the possible existence of at least two different, coexisting mechanisms for the production of time-variabilities in the ejection of HH jets.

As described in Sect. 4.2, the very high proper motions of the knots closest to the HH 34 source might be evidence that the 1400 yr period mode of the outflow variability of this jet might not be sinusoidal. However, the restricted information that we have about the ejection velocity rise that appears to have occurred over the last few decades does not allow us to determine the functional form of this mode in detail.

4.6. The numerical simulations

The numerical simulations that we have computed show that the ejection velocity histories deduced from the radial velocities of HH 34 and HH 111 do lead to jets with the observed characteristics. The HH 34S and HH 111V main bow shocks are well reproduced by the numerical models, and the structures of aligned knots observed at the bases of the jets are also reproduced at least in a qualitative way. We feel that this is a quite definite proof that at least some of the structures observed in HH 34 and HH 111 are indeed the result of a time-variability of the ejection velocity.

4.7. The transverse sizes of HH 34S and HH 111V

We find that by choosing an appropriate density for the surrounding environment, we are able to reproduce the widths of the HH 34S and HH 111V bow shocks. However, a problem with our models is that the environment of the outflows is likely to have been subjected to long-term perturbations due to the passage of many working surfaces (as shown by the $\sim 10^4$ yr dynamical timescales of the giant jets associated with these objects, see Devine et al. 1997 and Reipurth et al 1997b). Such perturbations are not included in our present simulations.

Therefore, it is not possible to derive any definite conclusions from the predicted and observed widths of HH 34S and HH 111V, and we are limited to saying that the widths of these objects can be reproduced with our models by choosing appropriate environmental parameters. However, the chosen parameters are unlikely to coincide with the real corresponding values for these HH jets, since the long-timescale perturbations that these outflows have inflicted on their environments are not included in our models.

4.8. Time-dependence of the ejection density

In our simulations, we have considered a time-independent density at the base of the jet. We find that with this assumption it is possible to obtain jets with characteristics that qualitatively agree with observations of HH 34 and HH 111.

However, it is of course possible that the ejection density is also varying as a function of time. Variations in the density by as much as an order of magnitude could be present, even if it is not possible to isolate them from the clearly detected velocity variabilities. The difficulty in detecting an ejection density time-variability comes from the fact that a variability in the ejection velocity leads to a strong position dependence of the density along the jet, as discussed by Raga & Cantó (1998).

It is therefore very difficult to isolate the density vs. position dependence which might result from a time-dependent ejection density from the one resulting from the existing ejection velocity time-variability. However, this is one of the interesting points that could be addressed from observations of HH jets, and clearly deserves further effort.

5. Conclusions

We have computed axisymmetric gasdynamic models with the time-dependent ejection velocities deduced from the position-dependent radial velocities of the HH 34 and HH 111 jets. From these models, we predict Hα maps that have quite strong qualitative and quantitative agreements with observations of these two jets. From this, we conclude that it is clear that at least some of the structures observed in HH 34 and HH 111 are indeed the result of an ejection velocity time-variability.

We have studied the periods, amplitudes, phases and functional forms of the modes of the ejection velocity time-variability. We find that the amplitudes of the modes are consistent with the ~ 120 km s^{-1} upper limit to the shock velocities deduced from the excitation of HH spectra.

Other interesting results are that it appears that up to three different modes are active at the current time, and that these modes have at least two different functional forms. These results suggest that at least two different mechanisms producing variabilities of the ejection velocity (with different amplitudes, periods and functional forms) might be active at the current time in HH 34 and HH 111.

These results are hard to understand at the present time, due to the lack of firm theoretical ideas about the production of time-dependent HH jets. However, they do provide important constraints for future jet collimation models that could evolve, e.g., as more advanced versions of time-dependent models such as the ones of Ouyed & Pudritz (1997) and Goodson et al. (1997, 1999).

Acknowledgements. This work was supported by CONACyT grants 34566-E and 36572-E. We thank Israel Díaz for his support with the new computer equipment with which the numerical simulations were carried out. We thank Bo Reipurth (the referee) for helpful comments on the first version of the manuscript.

References

Biro, S. 1996, MNRAS, 278, 990
Bührke, T., Mundt, R., & Ray, T. P. 1988, A&A, 200, 99
Cernicharo, J., & Reipurth, B. 1996, ApJ, 460, L57
Coppin, K. E. K., Davis, C. J., & Micono, M. 1998, MNRAS, 301, L10
Davis, C. J., Mundt, R., & Eislöffel, J. 1994, ApJ, 437, L55
Devine, D., Bally, J., Reipurth, B., & Heathcote, S. 1997, AJ, 114, 2095
Eislöffel, J., & Mundt, R. 1992, A&A, 263, 292
Eislöffel, J., & Mundt, R. 1997, AJ, 114, 280
Falle, S. A. E. G., & Raga, A. C. 1993, MNRAS, 261, 573
Falle, S. A. E. G., & Raga, A. C. 1995, MNRAS, 272, 785
Goodson, S. P., Winglee, R. M., & Böhm, K. H. 1997, ApJ, 489, 199
Goodson, S. P., Böhm, K. H., & Winglee, R. M. 1999, ApJ, 524, 142
Gredel, R., & Reipurth, B. 1994, A&A, 289, L19
Hartigan, P., Morse, J. A., Reipurth, B., Heathcote, S., & Bally, J. 2001, ApJ, 559, L157
Heathcote, S., & Reipurth, B. 1992, AJ, 104, 2193
Masciadri, E., Velázquez, P. F., Raga, A. C., Cantó, J., & Noriega-Crespo, A. 2002, 573, 260
Morse, J. A., Hartigan, P., Cecil, G., Raymond, J. C., & Heathcote, S. 1992, ApJ, 399, 231
Morse, J. A., Heathcote, S., Hartigan, P., & Cecil, G. 1993a, AJ, 106, 1139
Morse, J. A., Heathcote, S., Cecil, G., Hartigan, P., & Raymond, J. C. 1993b, ApJ, 410, 764
Nagar, N. M., Vogel, S. N., Stone, J. M., & Ostriker, E. C. 1997, ApJ, 482, L195
Ouyed, R., & Pudritz, R. E. 1997, ApJ, 484, 794
Raga, A. C., Noriega-Crespo, A., Reipurth, B., et al. 2002a, ApJ, 565, L29
Raga, A. C., de Gouveia Dal Pino, E., Noriega-Crespo, A., Mininni, P., & Velázquez, P. F. 2002b, A&A, in press
Raga, A. C., Sobral, H., Villagrán-Muniz, M., Navarro-González, R., & Masciadri, E. 2001, MNRAS, 324, 206
Raga, A. C., Navarro-González, R., & Villagrán-Muniz, M. 2000, RMxAA, 36, 67
Raga, A., & Cantó, J. 1998, RMxAA, 34, 73
Raga, A. C., & Noriega-Crespo, A. 1998, AJ, 116, 2943

Raga, A. C., Böhm, K. H. & Cantó, J. 1996, RMxAA, 32, 161
Raga, A. C., Cantó, J., Binette, L., & Calvet, N. 1990, ApJ, 364, 601
Reipurth, B. 1989, Nature, 340, 42
Reipurth, B., Heathcote, S., Morse, J. A., Hartigan, P., & Bally, J. 2002, AJ, 123, 362
Reipurth, B., Yu, K. C., Heathcote, S., Bally, J., & Rodríguez, L. F. 1999, AJ, 120, 1449
Reipurth, B., Yu, K. C., Rodríguez, L. F., Heathcote, S., & Bally, J. 1999, A&A, 352, L83
Reipurth, B., Hartigan, P., Heathcote, S., Morse, J. A., & Bally, J. 1997a, AJ, 114, 757
Reipurth, B., Bally, J., & Devine, D. 1997b, AJ, 114, 757
Reipurth, B., Raga, A. C., & Heathcote, S. 1992, ApJ, 392, 145
Reipurth, B., & Heathcote, S. 1992, A&A, 257, 693
Reipurth, B., Bally, J., Graham, J. A., Lane, A. P., & Zealey, W. J. 1986, A&A, 164, 51
Riera, A., López, R., Raga, A. C., Anglada, G., & Estalella, R. 2001, RMxAA, 37, 147
Rosado, M., Raga, A. C. & Arias, L. 1999, AJ, 117, 462
Sobral, H., Villagrán-Muniz, M., Navarro-González, R. & Raga, A. C. 2000, App. Phys. Lett., 77, 3158
van Leer, B. 1982, ICASE Report Nos. 82-30
Velázquez, P. F., Sobral, H., Raga, A. C., Villagrán-Muniz, M., & Navarro-González, R. 2001, RMxAA, 37, 87
Völker, R., Smith, M. D., Suttner, G., & Yorke, H. V. 1999, A&A, 343, 953